Imaging Neutral Particle Analyzer engineering design and installation for the ASDEX Upgrade tokamak

J. Garcia-Dominguez[1,2], J. Rueda-Rueda[1,2], E. Viezzer[1,2], P. A. Schneider[4], J. Ayllon-Guerola[2,3], M. Garcia-Munoz[1,2], J. Hidalgo-Salaverri[2,3], A. Mancini[1,2], M. Videla[1,2], A. Herrmann[4] and the ASDEX Upgrade Team

[1] *Department of Atomic, Molecular and Nuclear Physics, University of Seville, Seville, Spain*
[2] *Centro Nacional de Aceleradores (U. Sevilla, CSIC, J. de Andalucia), Seville, Spain*
[3] *Department of Mechanical Engineering and Manufacturing, University of Seville, Seville, Spain*
[4] *Max-Planck-Institut für Plasmaphysik, Garching, Germany*

***Abstract*— An Imaging Neutral Particle Analyzer (INPA) has been installed in the ASDEX Upgrade tokamak (AUG) to provide simultaneous measurements of the radial profile and the energy of the confined fast-ion population. The INPA diagnostic leverages the advantages of Neutral Particle Analyzers (NPA) and Fast-Ion Loss Detectors (FILD) by measuring charge exchange neutrals ionized by an ultra-thin carbon foil deflected into a scintillator by the local magnetic field.**

The design of this diagnostic has been developed under a series of constraints such as the lack of space and hazardous environment (high level of neutron and gamma radiation), the need of high precision in the alignment of the non-sequential optical system (with 6 optical axes) and the optimization of the scintillator plate (signal emitter). To this end, a modular and adjustable design has been pursued with several degrees of freedom to ensure precise positioning during the installation and optical calibration.

The induced electromagnetic and thermal stresses have been assessed and compared against the material limits of the detector, showing that no significant stress is expected for the system. The thermal analysis shows that the diagnostic scintillator can work efficiently during normal operation conditions. The CAD design, a comparison between the synthetic and real optical signals and the mechanical assessment (based on finite element analysis) are presented in this contribution.

***Index Terms*— ASDEX Upgrade tokamak, fast-ions, Imaging Neutral Particle Analyzer, Fast-Ion Loss Detectors, degrees of freedom.**

I. Introduction

A good fast-ion confinement is key for a self-maintained burning plasma. The loss of fast ions, due to several mechanisms [1], can jeopardize fusion performance and damage the tokamak first wall. Imaging Neutral Particle Analyzer (INPA) [2],[3] combines the working principles of the Fast-Ion Loss Detector (FILD) [4] and the Neutral Particle Analyzer (NPA) [5] diagnostics. INPA provides the energy and spatial location of the fast-ions (FI) population. This diagnostic can obtain these measurements with high phase-space resolution at kHz rate.

This paper is organized as follows: A detailed description of the diagnostic, including an overview of the mechanical design and the system installation, is presented in Section II. In Section III, the optical system is described, together with the simulations performed for its design and signal quality validation, and its calibration. Finally, in Section IV, the electro-mechanical and thermal assessments, performed to ensure the structural safety of the system, are described.

II. INPA Design Description

A. Mechanical design overview

The INPA diagnostic was installed in the AUG tokamak during 2021, specifically, in the upper horizontal port in sector 16, as shown in Figure 1, where an overall description of the system is presented. The commissioning and first operation of this detector is foreseen for the AUG experimental campaign 2022.

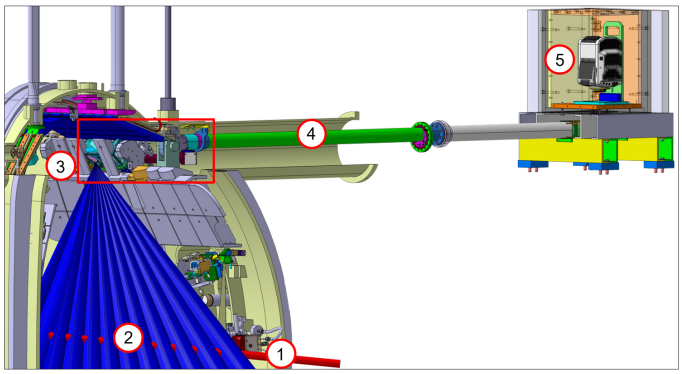

Fig. 1. Overall INPA design description: (1) NBI beam. (2) Intersection between lines of sight and NBI beam. (3) INPA head, see detailed view in Figure 2. (4) Tube with the optical system inside. (5) Phantom camera.

The diagnostic principle of the INPA detector relies on the charge exchange (CX) process between the neutral particles, injected by the Neutral Beam Injector (NBI) and ions in the plasma. The plasma ions retain their energy and momentum while neutralized in the CX process. These neutrals can travel

freely in the magnetic field and enter the INPA head (Figure 2), where they are collimated, ionized, and dispersed onto a scintillator plate. The light emitted by the scintillator is monitored by sensors located ex-vessel. This can be described in more detail using Figure 1 as a reference: the neutrals injected by the NBI (1) undergo the CX process due to interaction with the ionized plasma in the region marked as (2). The CX neutral flux will then be captured by a collimator, ionized by a carbon foil, and dispersed onto a scintillator plate located into the detector head (3). Further details of this process are given in Figure 2. Finally, the light emitted by the scintillator is guided by an optical path (4) up to the sensors (Phantom Camera and Photomultipliers (PMT)) located ex-vessel. The camera is fixed in a shielding box designed for minimizing the effects of magnetic fields and neutrons.

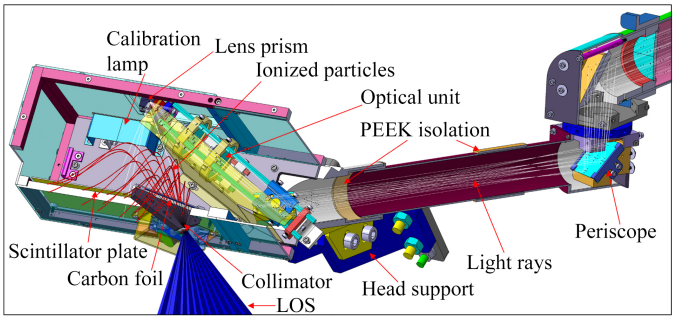

Fig. 2. Detailed section view of number 3 in Figure 1, INPA head design according to its performance.

Fig. 2 shows in detail the internal process happening inside the INPA head. When neutrals enter the head, after the collimation, they get ionized by an ultra-thin carbon foil of 20 nm thickness and 56 mm length (see Figure 3). Due to the local magnetic field, ir changes its straight trajectory to an orbital one. Ionized particles collide in different areas of a scintillator plate, depending on their radial profile and energy. The scintillator used, shown in Figure 3, is TG-Green [7], similar to the ones used in the AUG FILD detectors.

An optical system carries the light emitted by the scintillator plate out of the vessel. This system, consisting of a set of lenses and mirrors, provides signal with high spatial resolution. The light will then split into two sensors: a Phantom camera, which is expected to measure up to 10 kHz with high signal-to noise ratio and good spatial resolution, <1mm and below 3mm (12 keV and 7cm); and an array of PMT, for a high temporal resolution response up to 1 MHz.

The diagnostic mechanical design is highly restricted due to numerous constraints such as the lack of available space, the necessity of keeping gaps with respect to other systems (to avoid electric arcs) and the assembly/installation process. Also, high precision during the installation and calibration processes is required and, for this reason, several components of the system have been designed to provide enough degrees of freedom to assure flexibility and good accuracy during these processes.

Finally, it is important to highlight that the signal quality depends on the size of the scintillator plate and its distance to the first lens. These factors are correlated to the size of the INPA head and, therefore, a compromise must be reached between the dimensions of this element and the space limitations.

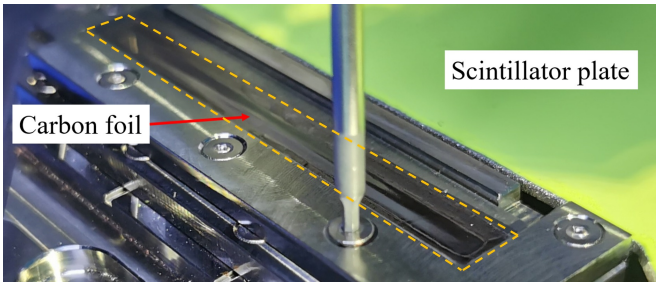

Fig. 3. Ultra-thin carbon foil, (20 nm x 56 mm x 6mm) and scintillator plate (yellow surface, TG-Green).

B. System installation

The INPA installation process requires a modular system divided into different sections to be assembled in different locations, allowing a proper optical calibration that will be described in the next section.

Inside the vessel, the bottom part of the periscope with the red tube, shown in Figure 2, was mounted and fixed with the upper part of the periscope, introduced with the long green tube, Figure 1, from the ex-vessel side.

For the mechanical alignment, following procedure was to allocate lasers inside the INPA head, mimicking the straight path of CX neutral towards the collimator. These lasers are oriented in the same plane as the collimator and the NBI beam. The INPA head is properly aligned when the lasers match with the NBI line (position indicated by a white rope in Figure 4). In this figure, the red dot coming from the laser coincides with the NBI injection line showing a good agreement in the alignment. The blue cones are a CAD figure superimposed to the image, representing the view of the diagnostic.

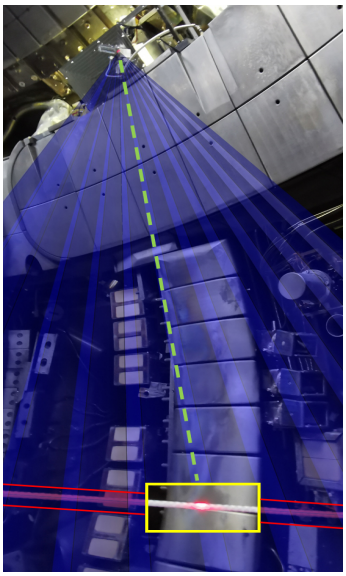

Fig. 4. Match between the NBI injection line and lasers positioned inside the INPA head during the installation/alignment process.

III. Optical system

A. Description

The design of the INPA optical system is determined by the space limitations and the difficult assembly process needed to install this diagnostic. The resulting path allowing the transmission of the light from the scintillator (in-vessel) to the out-vessel acquisition systems (camera and PMTs) consists of 6 non-sequential optical axes and different optical components. Specifically, the optical array uses a modified prism, 5 lenses, 3 mirrors and a beam splitter.

The maximum distance available between the scintillator plate and the first lens (see Figure 2) is less than 9 cm, due to space restrictions. For this reason, a customized prism, shown in Figure 5, was designed and manufactured, allowing a field of view (FOV) that covers the scintillator plate. The use of this element allows for a FOV diameter of 140 mm, at expenses of introducing a barrel distortion, an effect that will be discussed later, (see subsection B).

The optimized diameter of the collimator pinhole is 3 mm, a parameter that defines the size of the expected resolution signal in the scintillator plate. Near the optical axis, the resolution will be below to 1mm. The position of this axis has been optimized where the maximum signal is expected in the experiment, being that position the FOV center. And the borders, it resolution decreases to 3mm.

The optical aperture has been optimized by virtue of the stop diameter in 40mm (diameter which limits the solid angle of the rays passing through the optical system from an on-axis object point). This is the diameter of the red tube shown in Figure 2, connecting the INPA head to the periscope, which is limited by spatial constraints.

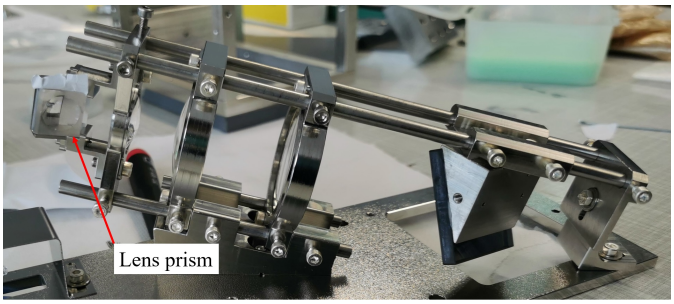

Fig. 5. Lens system inside the INPA head. Lens prism is shown on the left, being the first of the optical system.

B. Optical simulations

For the design of the INPA optical system, simulations were performed using the software Zemax [8]. The expected optical resolution for the detector is 1 mm at the optical axis and 3 mm at the FOV border. This is shown in Figure 6 where a comparison between the input and output signals is presented. The input signal consists of several 3 mm emission areas with different gaps between them and the simulated output signal shows that the spots can be disentangled even at the borders of the FOV (where the resolution is minimal).

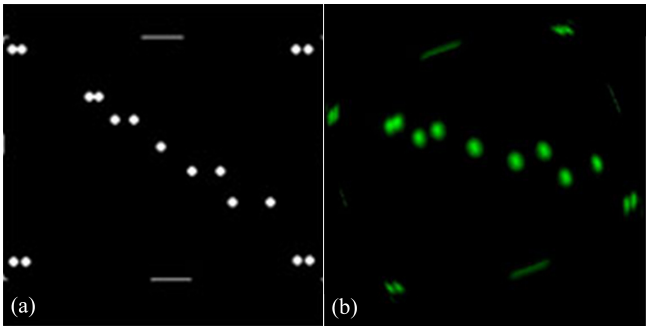

Fig. 6. Input (a) and output (b) signal in optic simulation.

To estimate the spherical distortion of the INPA optics with respect to the optical axis, a 1 cm spaced grid image was used to be compared in Zemax. The results are shown in Figure 7, where the distortion is plotted against the experimental measurements performed at the laboratory using the actual device. The red dot in the grid is the image center (optical axis). As the values move away radially from the center in the scintillator plane, the percentage of distortion increases as predicted by Zemax. This distortion was obtained using $Dist=(d-d_r)/(d_r)$, where d is the distance to the selected point in the grid (real distance) and d_r the one in the distorted image. This comparison shows a good agreement between the simulations and the experiments, indicating that the spherical distortion can be corrected during the post-processing data analysis.

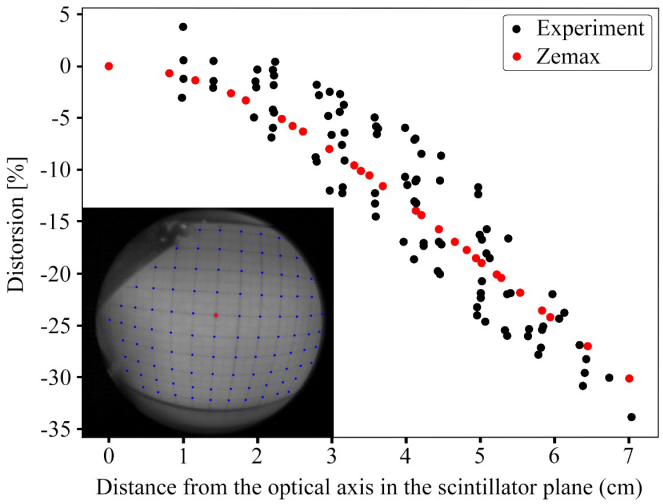

Fig. 7. Comparison between the simulated and experimental spherical distortion, increasing with the distance to the FOV center, (distance from the red dot, optical axis, to the border of the image).

C. Optical calibration

To calibrate the INPA optical system, an out-vessel laser has been positioned at the camera sensor location, coinciding with the optical axis, following the reverse optical path of the signal (3 meters length). As shown in Figure 8, the laser reaches the scintillator plate (red dot at Figure 8 right) exactly at the theoretical position of the optical axis (red dot at Figure 8 left).

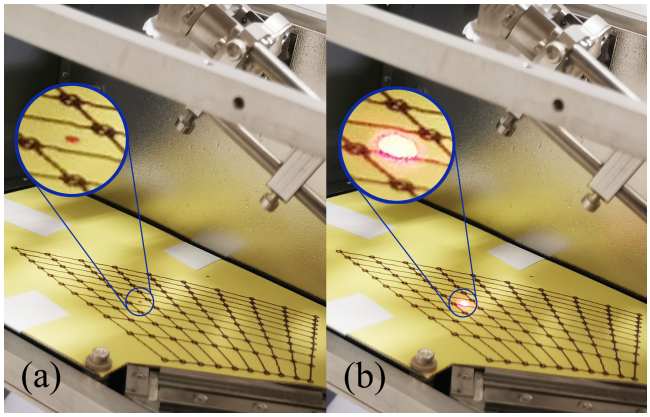

Fig. 8. Optical axis position: theoretical (a) marker red dot vs. experimental, laser red dot (b).

Finally, in Figure 9, a comparison between the detector synthetic signal (simulated INPA signal and strike map) and the real signal (obtained after the system assembly and installation) is presented.
As the result for the optical alignment, Figure 9 shows the comparison between the synthetic signal (left), used as base model for the optical design, and the real image (right), obtained in the final optical alignment, after the assembly process with a Phantom camera. The right image is a sketch of the strike map fixed over the scintillator plate, to see the correlation obtained. It is expected to reach signals similar to the theoretical one.

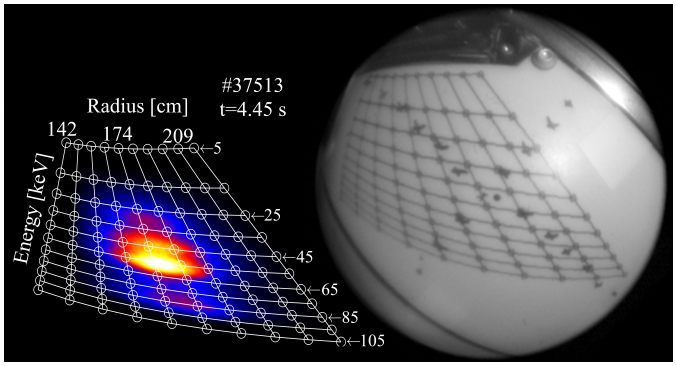

Fig. 9. Comparison between the synthetic signal used as base model (left) and the real image obtained in the final optical alignment after the assembly process, with a strike map figure as the object (right).

IV. Structural Integrity

The structural integrity of the INPA system has been assessed using Finite Element Analysis (FEA) to ensure a safe operation of the system under the worst-case scenarios. Joints between parts have been considered as the same in reality. Most of the components of the detector are made of stainless steel AISI 316. Its mechanical properties are shown in Table 1.

TABLE I
SS316 STAINLESS STEEL MATERIAL PROPERTIES

Density	7850 kg/m^3
Specific heat capacity	404 J/kgK (@100ºC)
Conductivity	14.7 W/mK (@100ºC)
Thermal expansion	$15 \cdot 10^{-6}$ /K
Yield strength	270 MPa
Melting temperature	1370ºC

A. Electro-mechanical assessment

An electro-magnetic model has been developed to study the forces acting on the system due to induced currents during the current ramps [9] feeding all the poloidal and toroidal coils. The current evolution in the coils was obtained from the reference AUG discharge #39613. Figure 10 shows that the maximum stress (equivalent Von Mises stress) obtained during a complete shot is around 2 MPa. The stress, as expected, concentrates in the head and periscope supports and, according to the results shown, can be neglected for being too low compared to the material yielding strength presented in Table 1.

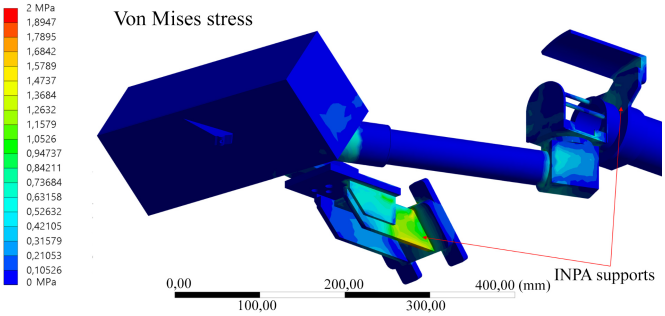

Fig. 10. Maximum Von Mises stress produced by transient magnetic forces induced by the coil current ramps.

B. Thermal assessment

The INPA diagnostic head is facing the plasma and, therefore, it will be subject to relatively high thermal loads. Graphite protections cover the INPA front side exposed to radial heat fluxes (Figure 11).
To evaluate the heat flux parallel to the magnetic field lines, the exponential λ_q model [10],[11] has been used. The heat flux is estimated from discharge #36524 at 2.30s, where it reaches the maximum value of 1.99 W/mm^2. Using a conservative approach to explore the limits of the system [12],[13], this maximum heat flux has been applied to the plasma facing surfaces and extended during a simulation of 10 seconds.

Fig. 11. INPA head being protected from the radial heat flux by three graphite protections.

The maximum temperature found in the INPA components facing the plasma is shown in Figure 12. A maximum value close to 1000 ºC is found in a very small region of a non-structural cover plate. This temperature is not critical compared to the material limits, especially considering that the case analyzed is very conservative.

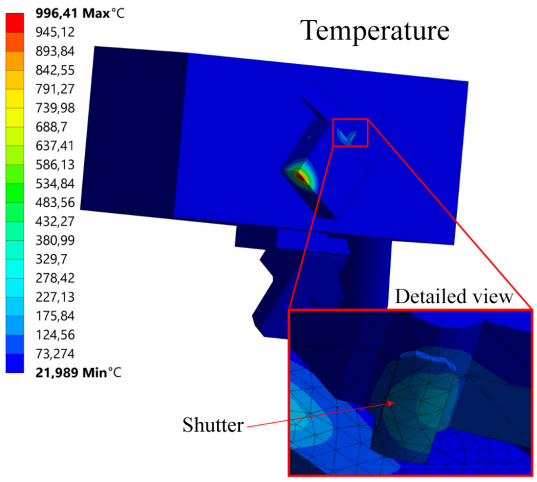

Fig. 12. Maximum temperature values induced by the parallel heat flux during transient thermal assessment.

The stress induced due to the temperature gradients is shown in Figure 13. It can be observed that, overall, the stress is low compared to the material limits and that some local stress concentration points can be found in the cover plate. However, this maximum stress is not critical compared to the material yielding stress.

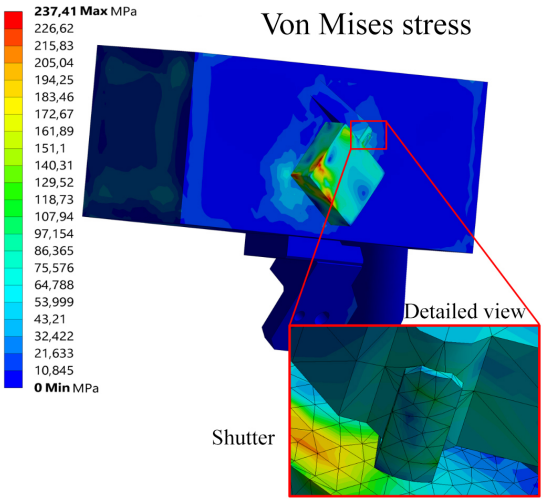

Fig. 13. Maximum Von Mises stress induced by the parallel heat flux during transient thermal assessment.

The time evolution of the temperature and the maximum stress are represented in Figure 14. As expected, the temperature continuously increases during the plasma pulse evolution reaching a maximum value of 1000 ºC approximately. On the other hand, the stress reaches the maximum value at the beginning of the pulse and stabilizes at around 250 MPa, due to thermal dissipations around the cover. As mentioned before, both maximum values of the temperature and stress are not critical for the system, and it can be concluded that the diagnostic is thermally protected and structurally safe.

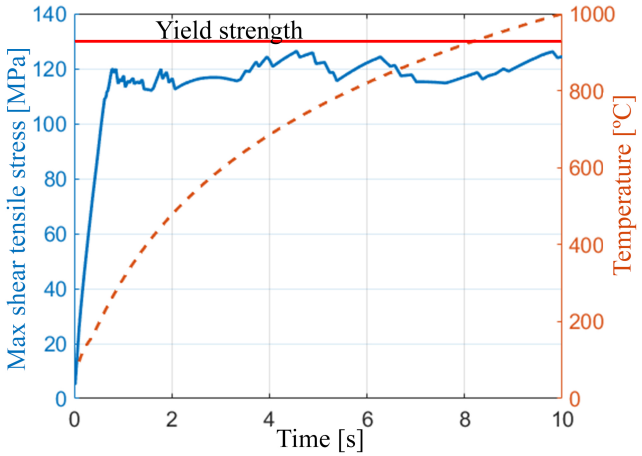

Fig. 14. Maximum thermal stress and temperatures values, during the transient thermal assessment.

V. Conclusions

The design and installation of the INPA diagnostic at ASDEX Upgrade is presented in this work. The mechanical design of the system allows for high precision in the optical calibration and system installation, guaranteeing an optimal operation. Simulations foresee good agreement between the synthetic signal and the expected measurements. This will be verified in the commissioning and first operation phase, planned during the AUG experimental campaign 2022.

The INPA diagnostic is expected to withstand conservative thermal loads, as estimated using parallel heat flux simulations. The induced forces due to the coil current ramps are admissible. The behavior of the detector during a disruptive event will be presented in another publication.

VI. Acknowledgements

Special thanks to Wolfgang Zeidner, Wolfgang Popken and Michael Ebner for the infinite help and support in the development and installation of this diagnostic.

This project received funding from the European Research Council (ERC) under the European Union's Horizon 2020 research and innovation programme (Grant Agreement No. 805162) and the Spanish Ministerio de Ciencia, Innovación y Universidades (Grant No. FPU19/02486).

VII. References

[1] W.W. Heidbrink, "The behaviour of fast ions in tokamak experiments" Nucl. Fusion, vol 34, pp 541-615, Dec. 1995.

[2] Du, X. D., "Development and verification of a novel scintillator-based, imaging neutral particle analyzer in DIII-D tokamak" Nucl. Fusion, vol 58, 082006, Aug. 2018.

[3] J. Rueda-Rueda, "Design and simulation of an imaging neutral particle analyzer for the ASDEX Upgrade tokamak" Rev. Sci. Instrum, vol 92, 043554, Mar. 2021.

[4] M. Garcia-Munoz, “Scintillator based detector for fast-ion losses induced by magnetohydrodynamic instabilities in the ASDEX upgrade tokamak” Rev. Sci. Instrum., vol 80, 053503, Mar. 2009.
[5] S. S. Medley, “Contemporary instrumentation and application of charge exchange neutral particle diagnostics in magnetic fusion energy experiments” Rev. Sci. Instrum., vol 79, 011101, Jan. 2008.
[6] H. Hutchinson, “Principles of Plasma Diagnostic”, 2nd ed. Cambridge University Press, 2002, pp. 322.
[7] M. C. Jimenez-Ramos, “Characterization of scintillator materials for fast-ion loss detectors in nuclear fusion reactors” Nucl. Instrum. Methods Phys. Res, vol 332, pp. 216- 219, Aug. 2014.
[8] Quingyan Li, “Design and alignment to off-axis reflection beam expanding and contracting optical system” Microw. Opt. Techn. Let., vol 63, 32998, Oct. 2021.
[9] A. Mancini, “Mechanical and electromagnetic design of the vacuum vessel of the SMART tokamak” Fusion Eng. Des., vol 171, 112542, Oct. 2021.
[10] R. Mitteau, “Heat flux deposition on plasma-facing components using a convective model with ripple and Shafranov shift” J. Nucl. Mater, vol 266–269, pp. 798-803, Mar. 1999.
[11] T. Lunt, “Near- And far scrape-off layer transport studies in detached, small-ELM ASDEX upgrade discharges by means of EMC3-EIRENE,” Plasma Phys. Control. Fusion, vol 62, 105016, Jul. 2020.
[12] J. Hidalgo-Salaverri, “Thermo-mechanical limits of a magnetically driven fast-ion loss detector in the ASDEX Upgrade tokamak” Poster European Conference on Plasma Diagnostic (2021), Salamanca.
[13] J. Ayllon-Guerola, “Thermo-mechanical assessment of the JT-60SA fast-ions loss detector” Fusion Eng. Des. vol 167,112304, Jun. 2021.